Solution NMR Determination of the Anisotropy and Orientation of the Paramagnetic Susceptibility Tensor as a Function of Temperature for Metmyoglobin Cyanide: Implications for the Population of Excited Electronic States

Bao D. Nguyen, Zhicheng Xia, Deok Cheon Yeh, K. Vyas, Helen Deaguero, and Gerd N. La Mar*

Contribution from the Department of Chemistry, University of California, Davis, California 95616

Received July 20, 1998. Revised Manuscript Received November 12, 1998

Abstract: Comprehensive ^{1}H NMR assignments of the heme cavity proton resonances of sperm whale metmyoglobin cyanide have provided the dipolar shifts for nonligated residues which, together with the crystal coordinates of carbonyl myoglobin, allow accurate determination of both the anisotropies and orientation of the paramagnetic susceptibility tensor, χ, in the molecular framework. The resulting axial, $\Delta\chi_{ax} = 2.48 \times 10^{-8}$ m^3/mol, and rhombic anisotropy, $\Delta\chi_{rh} = -0.58 \times 10^{-8}$ m^3/mol, values at 25 °C determined from the most complete set of dipolar shifts are determined to 2% and 6% uncertainty, respectively, and agree well with theoretical estimates (Horrocks, W. D., Jr. and Greenberg, E. S. *Mol. Phys.* **1974**, *27*, 993−999). Numerically and spatially restricted input data sets lead to larger uncertainties in $\Delta\chi_{ax}$ and $\Delta\chi_{rh}$, but do not systematically bias the orientation of the tensor. Determination of the anisotropies and orientation over the temperature range 5−50 °C shows that the susceptibility tensor orientation is minimally influenced, with both anisotropies well-behaved, and with $\Delta\chi_{ax}$ exhibiting a temperature behavior close to that predicted for the system. The quantitative determination of the magnetic anisotropies over temperature allows the quantitative separation of contact and dipolar shifts for the iron ligands. The heme contact shifts reflect the expected dominant π spin density at pyrrole positions, but the meso-protons exhibit low-field contact shifts indicative of unpaired spin in a σ orbital. Such delocalized σ spin density could arise from either deformation of the heme from planarity or the loss of σ/π separation for the d_{xz}, d_{yz} orbitals when the major magnetic axis is tilted strongly from the heme normal as is experimentally observed. The observed anomalous temperature dependencies of the heme methyl and axial His ring contact shifts, as well as that of the rhombic anisotropy, are all consistent with thermal population of the excited orbital state. The limitations for quanitatively determining the excited orbital state energy separation from the available NMR data are discussed.

Introduction

The potential unique and significant information content of the hyperfine shifts, δ_{hf}, for paramagnetic hemoproteins resulted in making myoglobin, Mb,[1] one of the earliest and most extensively studied proteins by NMR.[2] Of the various paramagnetic oxidation/spin states, the low-spin, ($S = {}^1/_2$) cyanomet form was the candidate of choice because of the excellent resolution and narrow lines even for resonances close to the iron.[3] There are two potential contributions to δ_{hf}, as given by[4,5]

$$\delta_{hf} = \delta_{con} + \delta_{dip} \tag{1}$$

The contact contribution, δ_{con}, results from direct delocalization of the metal unpaired spin onto the ligands of the iron, the heme, and ubiquitous proximal His and is given for nucleus j by

$$\delta_{con}{}^{j} = \frac{(A^j/h)}{3\beta\gamma/2\pi}\left(\frac{\chi_{xx}}{g_{xx}} + \frac{\chi_{yy}}{g_{yy}} + \frac{\chi_{zz}}{g_{zz}}\right) \tag{2}$$

where χ_{ii}, g_{ii} ($ii = xx, yy, zz$) are the components of the diagonal paramagnetic susceptibilty $\tilde{\chi}$, and spectroscopic splitting $\tilde{\mathbf{g}}$ tensors, respectively, in the magnetic coordinate system, μ_o is permeability of vacuum, β is the Bohr magneton, and γ is the magnetogyric ratio of the nucleus. A^j/h measures the amount of spin density, ρ_j, for nucleus j, via the relationship,[5,6] $A^j = Q\rho_j$, where Q is a constant; low-spin ferrric hemes have the lone unpaired spin in a π-bonding d orbital. The contact shifts for nonequivalent nuclei map out the nature of the π molecular

* Correspondence author. E-mail: lamar@indigo.ucdavis.edu. Phone: (530) 752-0958. FAX: (530) 752-8995.

(1) Abbreviations used: DSS, 2,2-dimethyl-2-silapentane-5-sulfonate; Mb, myoglobin; MbCO, carbonmonoxymyoglobin; COSY, 2D correlation spectroscopy; metMbCN, cyanomet myoglobin; NMR, nuclear magnetic resonance; NOE, nuclear Overhauser effect; NOESY, two-dimensional nuclear Overhauser spectroscopy; TOCSY, two-dimensional total correlation spectroscopy; WEFT, water-eliminated Fourier transform.

(2) Wüthrich, K. *Struct. Bonding* **1970**, *8*, 53−121.; Phillips, W. D. In *NMR of Paramagnetic Molecules*; LaMar, G. N., Horrocks, W. D., Jr.; Holm, R. H., Eds.; Academic Press: New York, 1973; pp 421−478; Morrow, J. J.; Gurd, F. R. N. *CRC Crit. Rev. Biochem.* **1973**, *3*, 221−272.

(3) Wüthrich, K.; Shulman, R. G.; Peisach, J. *Proc. Natl. Acad. Sci. U.S.A.* **1968**, *60*, 373−380; Wüthrich, K.; Shulman, R. G.; Yamane, T.; Wyluda, B. J.; Hugli, T. E.; Gurd, F. R. *J. Biol. Chem.* **1970**, *245*, 1974−1953; Sheard, B.; Yamane, T.; Shulman, R. G. *J. Mol. Biol.* **1970**, *53*, 35−48.

(4) Kurland, R. J.; McGarvey, B. R. *J. Magn. Reson.* **1970**, *2*, 286−301.

(5) Bertini, I.; Luchinat, C. *NMR of Paramagnetic Molecules in Biological Systems*; Benjamin Cummings Publishing Co.: Menlo Park, 1986.

(6) La Mar, G. N. In *NMR of Paramagnetic Molecules*; LaMar, G. N., Horrocks, W. D., Jr.; Holm, R. H., Eds.; Academic Press: New York, 1973; pp 85−126.

10.1021/ja982555o CCC: $18.00
Published on Web 12/19/1998

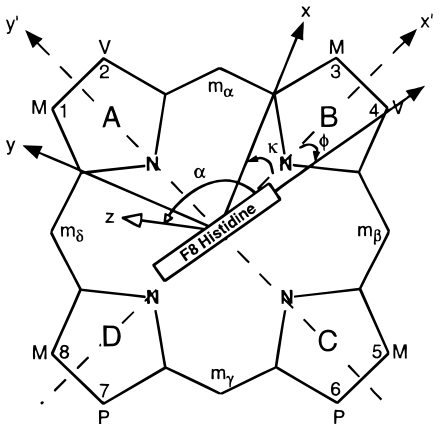

Figure 1. Schematic representation of the pseudosymmetric, iron-centered coordinate system, x', y', z' (R, θ', Ω') defined by the crystal coordinates of MbCO, and the magnetic axes, x, y, z (R, θ, Ω), in which the paramagnetic susceptibility tensor, $\boldsymbol{\chi}$, is diagonal. The two coordinate systems are related by the Euler angles rotation, $\Gamma(\alpha,\beta,\gamma)$, via $[x,y,z] = [x',y',z']\ \Gamma(\alpha,\beta,\gamma)$, where β is the angle between major magnetic axis, z, and the heme normal, z' (magnitude of the tilt of the major axis), α is the angle between the projection of the z axis on the heme plane and the x' axis (direction of the tilt of the major magnetic axis), and $\kappa \approx \alpha + \gamma$ defines the projection of the rhombic magnetic axes, x, y, on the heme plane relative to x', y'. ϕ defines the angle between the axial His plane and the N_B-Fe-N_c vector. [Note: The reference axes, x', y', z', have been rotated by 45° compared to previous studies from this lab,[10,14,25,26] and α defined with respect to the $+x'$, rather than $-x'$ axis, to conform with other works; this leads to changes in the three Euler angles β(new) = β(old); α(new) = α(old) + 135°; κ(new) = κ(old) − 45°.

orbital(s) containing the unpaired spin and hence are of considerable interest in describing the iron−heme and iron−His π bonding.[6−8]

The second contribution to δ_{hf} is from the dipolar or through-space interaction,[4,5] δ_{dip}, arises from anisotropy in the paramagnetic susceptibility tensor, and influences both ligated and nonligated residue signals according to the relationship

$$\delta_{dip} = (12\pi N_A)^{-1}[\Delta\chi_{ax}(3\cos^2\theta' - 1)R^{-3} + {}^3/_2\Delta\chi_{rh}(\sin^2\theta'\cos 2\Omega')R^{-3}]\Gamma(\alpha,\beta,\gamma) \quad (3)$$

where $\Delta\chi_{ax} = \chi_{zz} - {}^1/_2(\chi_{xx} + \chi_{yy})$, $\Delta\chi_{rh} = \chi_{xx} - \chi_{yy}$, R, θ', Ω'-(x',y',z') are the polar (Cartesian) coordinates of a proton in an arbitrary, iron-centered coordinate system, and $\Gamma(\alpha,\beta,\gamma)$ is the Euler rotation matrix that converts the arbitrary coordinate system,[9,10] into the magnetic coordinate system, R, θ, $\Omega(x,y,z)$ (Figure 1). The dipolar shifts due to delocalized spin density to a nucleus vanishes for a proton.[5] Thus, δ_{dip} contains valuable information on the magnitude of the anisotropies, which relate to the electronic structure of the heme iron,[11,12] the orientation of the tensor which can be related to the orientations of both the axial His relative to the heme,[12,13] and the distortion of the Fe−CN vector from the heme normal,[10,14] and can serve as a valuable constraint in constructing molecular models by solution NMR.[15] For simple, well-isolated spin states, χ, and hence both δ_{dip} and δ_{con}, follow the Curie (T^{-1}) law. For the present $S = {}^1/_2$, iron(III), there are nearby orbital states such that both terms would be expected to deviate signficantly from the Curie law.[11]

On the basis of the reasonable assumption that the contact contribution dominates the heme hyperfine shift, it was shown early that the large π contact shifts for 1-CH_3 and 5-CH_3 and smaller shifts for 3-CH_3 and 8-CH_3 in metMbCN are consistent with the expectation where the π bonding of the axial His imidazole raises the d_{xz}, d_{yz} degeneracy.[12,13] Because of the approximate alignment of the His imidazole along the pyrrole **B**,**D** vector,[16] the lone iron spin resides primarily in d_{xz} which can delocalize spin only to pyrrole A (1-CH_3) and pyrrole C (5-CH_3). However, since the spacing between d_{xz} and d_{yz} is comparable to kT,[11] the temperature dependence of the methyl contact shifts is expected to deviate from the simple Curie law due to the increased unpaired spin population of d_{yz}, which, at the high-temperature limit, should lead to comparable spin density at all four pyrroles. Such deviations from Curie law, in fact, are quite general among low-spin ferric hemoproteins,[17−21] with the methyl with larger shifts exhibiting larger slopes than T^{-1} (hyper-Curie), whereas the methyl with the smallest contact shifts show slopes much weaker than T^{-1} (hypo-Curie) or, in many cases, negative slopes or "anti-Curie" behavior. Modeling the temperature dependence of heme methyl ^1H and ^{13}C contact shifts on the basis of this model has generated estimates of the splitting[18−21] between d_{xz} and d_{yz} orbitals.

The difficulties in analyzing deviations from Curie behavior of heme methyl shifts in terms of orbital spacing are that the temperature dependencies of neither δ_{dip} nor δ_{con} are known for a single state and it is not realistic to assume a strict Curie law in light of theoretical considerations.[11] Moreover, the temperature dependencies of both $\Delta\chi_{ax}$ and $\Delta\chi_{rh}$ would have to be known. Last, thermal population of excited orbital states should lead to systematic anomalous temperature dependence for δ_{con} for the axial His as well as the heme and for δ_{dip} as influenced by χ_{rh} (see below). It is therefore clear that the first step in such an analysis requires the quantitative separation of δ_{hf} into δ_{con} and δ_{dip} *as a function of temperature*. Since any proton that exhibits nonzero δ_{con} (heme and axial His) also likely exhibits nonzero δ_{dip}, it is also obvious that the process can be initiated only by *first providing a quantitative description of* δ_{dip}, which is the only term that contributes to δ_{hf} for nonligated residues near the heme. Recent progress in the extension of 2D NMR methods[22−24] to low-spin ferric hemo-

(7) LaMar, G. N.; Walker, F. A. *The Porphyrins*; Dolphin, D., Ed.; Academic Press: New York, 1979, Part IV-B; pp 61−157.
(8) Walker, F. A.; Simonis, U. *Biol. Magn. Reson.* **1993**, *12*, 133−274.
(9) Williams, G.; Clayden, N. J.; Moore, G. R.; Williams, R. J. P. *J. Mol. Biol.* **1985**, *183*, 447−460.
(10) Emerson, S. D.; La Mar, G. N. *Biochemistry* **1990**, *29*, 1556−1566.
(11) Horrocks, W. D., Jr.; Greenberg, E. S. *Biochim. Biophys. Acta* **1973**, *322*, 38−44; Horrocks, W. D., Jr.; Greenberg, E. S. *Mol. Phys.* **1974**, *27*, 993−999.
(12) Shulman, R. G.; Glarum, S. H.; Karplus, M. *J. Mol. Biol.* **1971**, *57*, 93−115.
(13) Traylor, T. G.; Berzinis, A. P. *J. Am. Chem. Soc.* **1980,** *102*, 2844−2846.
(14) Rajarathnam, K.; La Mar, G. N.; Chiu, M. L.; Sligar, S. G. *J. Am. Chem. Soc.* **1992**, *114*, 9048−9058.
(15) Feng, Y. Q.; Roder, H.; Englander, S. W.; Wand, A. J.; Di Stefano, D. L. *Biochemistry* **1989**, *28*, 195−203; Banci, L.; Bertini, I.; Bren, K. L.; Cremonini, M. A.; Gray, H. B.; Luchinat, C.; Turano, P. *J. Biol. Inorg. Chem.* **1996**, *1*, 117−126 and references therein.
(16) Kuriyan, J.; Wilz, S.; Karplus, M.; Petsko, G. A. *J. Mol. Biol.* **1986**, *192*, 133−154.
(17) Satterlee, J. D. *Annu. Rep. NMR Spectrosc.* **1987**, *17*, p 80−178; Bertini, I.; Turano, P.; Villa, A. J. *Chem. Rev.* **1993**, *93*, 2833−2932; Yamamoto, Y. *Annu. Rep. NMR Spectrosc.* **1998**, *36*, 1−77.
(18) Turner, D. L. *Eur. J. Biochem.* **1993**, *211*, 563−568; Turner, D. L. *Eur. J. Biochem.* **1995**, *227*, 829−837.
(19) Brennan, L.; Turner, D. L. *Biochim. Biophys. Acta* **1997,** *1342*, 1−12.
(20) Shokhirev, N. V.; Walker, F. A. *J. Phys. Chem.* **1995**, *99*, 17795−17804.
(21) Banci, L.; Bertini, I.; Luchinat, C.; Pierattelli, R.; Shokhirev, N. V.; Walker, F. A. *J. Am. Chem. Soc.* **1998**, *120*, 8472−8479.
(22) Yu, L. P.; La Mar, G. N.; Rajarathnam, K. *J. Am. Chem. Soc.* **1990**, *112*, 9527−9534.
(23) Qin, J.; La Mar, G. N. *J. Biomol. NMR* **1992**, *2*, 597−618.

proteins has provided the δ_{dip} for numerous paramagnetically shifted protons of sperm whale metMbCN[10,14] and a number of its point mutants.[25,26] Using the crystal structure for R, θ', Ω' (eq 3) of a structural homologue, allowed simultaneous estimation of both the anisotropies, $\Delta\chi_{ax}$, $\Delta\chi_{rh}$, and orientation of the magnetic axes.[10,14,25,26] However, neither a complete data set has been used to determine the anisotropies and orientation of the axes, nor have the uncertainties in the parameters been ascertained on which an informative temperature study can be based.

A more quantitative description of the magnitude of the anisotropies and orientation of the tensor in metMbCN has recently taken an unrelated, but equally important, interest. Detailed studies of the residual $^1H-^{15}N$ dipolar contributions to the backbone $^{15}N-^1H$ scalar couplings for metMbCN partially oriented in a strong magnetic field[27] indicated the potential for novel information on slow collective motions involving whole helices in this protein.[28] Questions, however, have been raised[29] on the interpretation based on potential uncertainties in both the anisotropies and on the orientation of $\Delta\chi$ in sperm whale metMbCN. Hence, a more comprehensive ^1H NMR study of the solution magnetic and electronic properties of metMbCN is clearly warranted to answer some of the questions raised.

The goals of the present study are to (1) extend the assignments to all of the significantly dipolar-shifted protons in sperm whale metMbCN, (2) evaluate the use of variable input data that is potentially differentiately influenced by protein mobility as input for determining the anisotropy and orientation of the paramagnetic susceptibility, (3) estimate the uncertainties in each of the determined parameters, (4) determine the temperature dependence of the anisotropy and orientation of the paramagnetic susceptibility tensors for direct comparison with theoretical predictions,[11] and by inference, (5) define the temperature dependence of the contact shifts for the heme and axial His as well as for $\Delta\chi_{rh}$ in the context of their interpretation in terms of the spacing of the $(d_{xy})^2(d_{xz})^2(d_{yz})$ and $(d_{xy})^2(d_{xz})(d_{yz})^2$ orbital states.

Experimental Section

Sample Preparation. Sperm whale myoglobin was purchased from Sigma Chemical Co. and used without further purification. Cyanometmyoglobin (metMbCN) samples were prepared by addition of 1.5 equiv of $K_3Fe(CN)_6$, followed by repeated dialysis against 50 mM phosphate buffer at pH 8.6 containing 50 mM NaCl, 10 mM KCN in either ^2H_2O or 90% H_2O/10% ^2H_2O (pH uncorrected for the isotope effect). The final protein concentration is ~5 mM.

^{1}H NMR Spectra. All of the ^1H NMR spectra were collected on an GE Omega 500 MHz ^1H NMR spectrometer. The chemical shifts were referenced to 2,2′-dimethyl-2-silapentane-5-sulfonate (DSS) through the water peak. The rapidly relaxing signals were selectively enhanced in WEFT spectra[30] where the slowly relaxing diamagnetic envelope was suppressed. Steady-state nuclear Overhauser (NOE) spectra were collected by the application of a 50-ms soft pulse with the decoupler on resonance and with off resonance to provide a reference, with a total recycle time of 100 ms as described previously.[31] NOESY,[32,33] TOCSY,[34] and magnitude COSY[35] spectra were collected over the temperature range 5−50 °C for the ^2H_2O sample with a spectral window of 27.0 kHz using 2048 t_2 points; 64 scans were collected for each of 512 t_1 increments, with mixing time $\tau_m = 50$ ms. The recycle time is 700 ms. The NOESY spectra were also collected at 25 and 35 °C over 10.0 kHz with $\tau_m = 100$ ms and a 1.0 s recycle time to observe the diamagnetic signals. The TOCSY spectra were collected at 25 and 35 °C over 10.0 kHz with a spin lock time of 50 ms and a 1.2 s recycle time using the MLEV-17 mixing scheme.[36] The COSY spectra were recorded in the magnitude mode over 12.0 kHz with a 700 ms recycle time. Solvent suppression, when required, was achieved by direct saturation in the relaxation delay period. The data were processed as previously described;[23] details are given in the figure captions.

Magnetic Axes Determination. The magnetic axes were determined as described in detail previously.[10,14] Experimental dipolar shifts, δ_{DSS}(obsd), for protons on nonligated residues for structurally conserved portions of the heme environment (relative to the reference crystal structure[16]) were used as input to search for the Euler rotation angles, α, β, γ, that transform the iron-centered pseudosymmetry coordinates[37] (x', y', z', or R, θ', Ω', (Figure 1)), readily obtained from the MbCO crystal coordinates,[16] into magnetic axes, x, y, z, by minimizing the error function

$$F/n(\Delta\chi_{ax}, \Delta\chi_{rh}, \alpha, \beta, \gamma) = \Sigma|\delta_{dip}(\text{obsd}) - \delta_{dip}(\text{calcd})|^2 \quad (4)$$

with δ_{dip}(calcd) given by eq 1, and where

$$\delta_{dip}(\text{obsd}) = \delta_{DSS}(\text{obsd}) - \delta_{DSS}(\text{dia}) \quad (5)$$

and δ_{DSS}(obsd) is the observed chemical shift referenced to DSS. δ_{DSS}(dia) is the shift in the isostructural diamagnetic MbCO complex,[38] or calculated for protons whose δ_{DSS}(dia) are not available by using δ_{DSS}(dia) $= \delta_{tetr} + \delta_{sec} + \delta_{rc}$, where δ_{tetr} is the shift in an unfolded tetra peptide;[39] δ_{sec} is the shift of an amino acid proton typical for α-helices, β-strands, coils, etc.;[40] and δ_{rc} is the heme-induced ring current shift.[41] Minimizing the error function F/n in eq 4 was performed over five parameters, $\Delta\chi_{ax}$, $\Delta\chi_{rh}$, α, β, and γ, by using the MbCO crystal coordinates, as described in detail previously,[10,14,25,26] and subsequent error analyses were performed with the Levenberg−Marguardt method with the boundaries of the error function, F/n, set equal to 95.4% of

(24) La Mar, G. N.; de Ropp, J. S. *Biol. Magn. Reson.* **1993**, *12*, 1−78.
(25) Rajarathnam, K.; Qin, J.; La Mar, G. N.; Chiu, M. L.; Sligar, S. G. *Biochemistry* **1993**, *32*, 5670−5680; Qin, J.; La Mar, G. N.; Cutruzzola, F.; Travaglini Allocatelli, C.; Brancaccio, A.; Brunori, M. *Biophys. J.* **1993**, *65*, 2178−2190; Rajarathnam, K.; Qin, J.; La Mar, G. N.; Chiu, M. L.; Sligar, S. G. *Biochemistry* **1994**, *33*, 5493−5501; Zhao, X.; Vyas, K.; Nguyen, B. D.; Rajarathnam, K.; La Mar, G. N.; Li, T.; Phillips, G. N. J.; Eich, R. F.; Olson, J. S.; Ling, J.; Bocian, D. F. *J. Biol. Chem.* **1995**, *270*, 20763−20774;
(26) Zhang, W.; Cutruzzolá, F.; Travaglini Allocatelli, C.; Brunori, M.; La Mar, G. N. *Biophys. J.* **1997**, *73*, 1019−1030; Nguyen, B., D.; Zhao, X.; Vyas, K.; La Mar, G. N.; Lile, R. A.; Brucker, E. A.; Phillips, G. N., Jr.; Olson, J. S.; Wittenberg, J. B. *J. Biol. Chem.* **1998** *273*, 9517−9526.
(27) Tolman, J. R.; Flanagan, J. M.; Kennedy, M. A.; Prestegard, J. H. *Proc. Natl. Acad. Sci. U.S.A.* **1995**, *92*, 9279.
(28) Tolman, J. R.; Flanagan, J. M.; Kennedy, M. A.; Prestegard, J. H. *Nat. Struct. Biol.* **1997**, *4*, 292.
(29) Bax, A.; Tjandra, N. *Nat. Struct. Biol.* **1997**, *4*, 254.
(30) Gupta, R. K. *J. Magn. Reson*. **1976**, *24*, 461−465.
(31) Emerson, S. D.; La Mar, G. N. *Biochemistry* **1990**, *29*, 1545−1555.
(32) Jeener, J.; Meier, B. H.; Bachmann, P.; Ernst, R. R. *J. Chem. Phys*. **1979**, *71*, 4546−4553.
(33) States, D. J.; Haberkorn, R. A.; Ruben, D. J. *J. Magn. Reson.* **1982**, *48*, 286−292.
(34) Braunschweiler, L.; Ernst, R. R. *J. Magn. Reson.* **1983**, *53*, 521−528.
(35) Bax, A.; Freeman, R.; Morris, G. J. *J. Magn. Reson.* **1981**, *42*, 164−168.
(36) Bax, A.; Davis, D. G. *J. Magn. Reson*. **1985**, *65*, 355−360.
(37) The reference coordinate system used previously[10,14,20,25,26] has been redefined to bring it into conformity with that used elsewhere, with the x', y' axes passing through the pyrrole N−Fe−N rather than meso−Fe−meso axis; moreover, α is defined as the angle between the projection of the z axis on the x',y' plane and the x' rather than the $-x'$ axis. The definition of β is unchanged, but leads to α(new) = α(old) + 135°, κ(new) = κ(old) −45°.
(38) Mabbutt, B. C.; Wright, P. E. *Biochim. Biophys. Acta* **1985**, *832*, 175−185; Dalvit, C.; Wright, P. E. *J. Mol. Biol.* **1987**, *194*, 313−327; Theriault, Y.; Pochapsky, T. C.; Dalvit, C.; Chiu, M. L.; Sligar, S. G.; Wright, P. E. *J. Biomol. NMR* **1994**, *4*, 491−504.
(39) Bundi, A.; Wüthrich, K. *Biopolymers* **1979**, *18*, 285−297.
(40) Wishart, D. S.; Sykes, B. D.; Richards, F. *J. Mol. Biol.* **1991**, *222*, 311−333.
(41) Cross, K. J.; Wright, P. E. *J. Magn. Reson.* **1985**, *64*, 240−231.

the confidence limit.[42] For the iron-ligated porphyrin and axial His, the hyperfine shift is obtained via

$$\delta_{hf}(\text{obsd}) = \delta_{DSS}(\text{obsd}) - \delta_{DSS}(\text{dia}) \quad (6)$$

which, in turn, yields the contact shift via eq 1. Estimates of δ_{dip} due to breakdown of the point dipole approximation are <0.1 ppm for the proton closest to a pyrrole β-carbon with 0.1% spin density; these contributions are completely negligible compared to the 5−10 ppm δ_{dip} due to the spin density on the iron.

Results

Assignments. The majority of the previously reported WT metMbCN assignments[10,14] were based on 2D NMR data in ^2H_2O by using the crystal structure as a guide to expected heme contacts. Thus, all but one nonlabile proton with $R_{Fe} < 6$ were assigned, but relatively few protons with $R_{Fe} > 7$ Å were identified. Subsequent work on mutant metMbCN had shown that assignments could, for the most part, be determined sequence specifically via standard backbone connections.[25,26,43] Our interest here is to assign all of the protons with either $\delta_{dip} > 1$ ppm or $R_{Fe} < 9$ Å by using the δ_{dip}(calcd) from the determined magnetic axes interactively to identify all such candidates. The "intermediate" magnetic axes served as remarkably accurate indicators of the expected shifts for such target protons, and the ultimate magnetic axes identified 122 such target protons. The general approach for making these assignments is given below and only spectral data relevant to assigning the last elusive proton close to the iron, the $C_\epsilon H$ of His64(E7), are shown. Other 2D NMR data, as well as the listing of δ_{DSS}(obsd), δ_{DSS}(dia), δ_{dip}(obsd), and δ_{dip}(calcd) are given in Supporting Information.

The fingerprint region of the TOCSY and NOESY spectra[43] reveals the characteristic backbone connectivities for three helical segments, I−III, with TOCSY-detected side chains as follows: I, $Leu_iAla_{i+1}AMX_{i+2}AMX_{i+3}AMX_{i+4}Ala_{i+5}$ that must arise from Leu89(F4)−Ala94(F9) with AMX_{i+4} corresponding to the backbone of the previously assigned axial His93(F8); II, $AMX_jGly_{j+1}Val_{j+2}Thr_{j+3}Val_{j+4}X_{j+5}Thr_{j+6}Ala_{j+7}Leu_{j+8}Gly_{j+9}$ that arises from His64(E7)−Gly73(E16) with AMX_j exhibiting the expected NOESY cross-peaks to the previously reported His64(E7) $C_\delta H$; and III, $AMX_kLeu_{k+1}X_{k+2}AMX_{k+3}Ile_{k+4}$ that is uniquely assigned to Phe103(G4)−Ile107(G8) with AMX_k exhibiting the expected NOESY cross-peaks to an aromatic ring. While the C-helix backbone could not be located, a TOCSY-detected Thr spin and a long-chain residue (six of the seven protons) with significant dipolar shifts exhibit NOESY cross-peaks to 4-vinyl and 5-CH_3 as expected for Thr39(C4) and Lys42(C7); the assignments are confirmed by the characteristic helical $\alpha_i - \beta_{i+3}$ NOESY cross-peak. The residues Phe43(CD1), Phe46(CD4), Phe33(B14) and Leu29(B10), His97(FG3), Ile99(FG5) have been assigned previously on the basis of unique TOCSY and/or NOESY connectivities to the heme.[14,31] The complete list of assigned signals is given in Supporting Information and includes the assignment of 109 of the 122, or 90%, of the target protons with $\delta_{dip} \geq 1$ ppm or $R_{Fe} \leq 9$ Å, as well as an additional 26 protons with $R_{Fe} > 9$ Å but with $\delta_{dip} > 0.5$ ppm. Target protons not assigned include five due to lability and six side-chain protons likely lost because of expected degeneracy, as well as the termini of two Leus that possess mobility. The complete listing of assignments and δ_{dip}(calcd) for target and other assigned residue protons are given in Supporting Information.

The elusive, relaxed, distal His64(E7) $C_\epsilon H$,[31] with dipolar contact primarily to other strongly relaxed protons, could be assigned by steady-state NOEs in ^1H_2O. The reference WEFT spectrum of metMbCN in ^1H_2O is shown in Figure 2B with the assigned, resolved heme and His E7 signals labeled. Saturating the His64(E7) $N_\epsilon H$ in Figure 2C results in NOEs to the previously assigned[31,44] Phe43(CD1) $C_\epsilon H$ and Val68(E11) $C_\gamma H_3$, as well as to an unassigned strongly relaxed proton with strong temperature-dependent chemical shift at 2.01 ppm that must originate from the His64(E7) $C_\epsilon H$. After location in ^1H_2O, it was possible to detect the expected weak His64(E7) $C_\epsilon H$ NOESY cross-peaks to the Val68(E11) $C_\gamma H_3$ in ^2H_2O, as shown in Figure 2D.

Magnetic Axes. The δ_{dip}(obsd) for a proton was used as input into the magnetic axes determination only if its value correlated with its slope in a Curie plot, which is a reasonable criterion for establishing that the proton has a fixed position relative to the heme;[10,14] 96 of the 109 assigned target protons satisfied this condition. A plot of δ_{dip}(obsd) vs Curie slope for all of the 109 assigned target protons with dipolar shifts is given in Supporting Information and reveals that the side-chain termini of Leu F4, Val E11, and IleG8 are mobile and exhibit changes in the mean orientation of the residue with temperature.[10,14] Last, the dipolar shifts for the side-chain protons of His E7 were omitted as input from all magnetic axes determinations because the side chain can be expected to exhibit slightly different orientations in metMbCN relative to MbCO. Five-parameter searches were carried out at 25 °C using a variety of subsets of the available δ_{dip}(obsd). The subsets were arranged as proximal side protons (sets P), proximal and distal protons (sets PD), remote protons from the iron (>8 Å; sets R) and protons near the iron (<8 Å; sets N). To differentiate among data that could be influenced by flexibility, data subsets included helix backbone protons (set 1), helix backbone and nonmobile helix side-chain protons (set 2), set 2 plus all suitable protons on the FG turn (set 3), set 2 plus all suitable protons on the CD turn (set 4), and set 2 plus all suitable protons on both turns FG and CD (set 5). The additional reference set labeled VT includes a representative 26 dipolar shifts which were used as input to generate the magnetic axes over a range of temperatures The identity and relevant spectral parameters for the protons in each data set are listed in Supporting Information.

The optimized Euler angles, α, β, and κ ($= \alpha + \gamma$), and anisotropies resulting from five-parameter searches at 25 °C are listed in Supporting Information. The excellent correlation of δ_{dip}(obsd) vs δ_{dip}(calcd) at 25 °C for the most extensive input data set (see below) is shown in Figure 3A; the data for His64(E7) are also plotted using open markers. The parameters for the 16 independent fits lead to highly clustered parameters with total range[37,45] $\alpha = 150 \pm 10°$, $\beta = 15.8 \pm 0.6°$, $\kappa = -10 \pm 5°$, $\Delta\chi_{ax} = (2.56 \pm 0.08) \times 10^{-8}$ m^3/mol and $\Delta\chi_{rh} = (-0.59 \pm 0.10) \times 10^{-8}$ m^3/mol and excellent residual error function, F/n, with the results summarized in Figure 4. The use of the most complete input data set, PD5, yields $\Delta\chi_{ax} = (2.48 \pm 0.03) \times 10^{-8}$ m^3/mol, or a ±1% uncertainty, and $\Delta\chi_{rh} = (-0.59 \pm 0.04) \times 10^{-8}$ m^3/mol, a ±7% uncertainty. Changes in the $\Delta\chi_{ax}$ by

(42) Shrager, R. I. *J. Assoc. Comput. Mach.* **1970**, *17*, 446−452; Press W. H.; Flannery, B. P.; Teukolsky, S. A.; Vetterling, W. T. In *Numerical Recipes*; Cambridge University Press: Cambridge, 1986, Chapter 15.

(43) Wüthrich, K. *NMR of Proteins and Nucleic Acids*; Wiley-Interscience: New York, 1986.

(44) Emerson, S. D.; Lecomte, J. T. J.; La Mar, G. N. *J. Am. Chem. Soc.* **1988**, *110*, 4176−4182.

(45) The units of magnetic anisotropy are given in S. I. units, in contrast to units used previously in this lab.[10,14,25,26] $\Delta\chi$s in ref 10 are converted to SI units multiplying by 4π; those in refs 14 and 25 are converted to SI units by multiplying $\Delta\chi_{ax}$ by $12\pi N_A$ ($N_A = 6.02 \times 10^{23}$) and $\Delta\chi_{rh}$ by $-8\pi N_A$, and those in ref 26 by 4π.

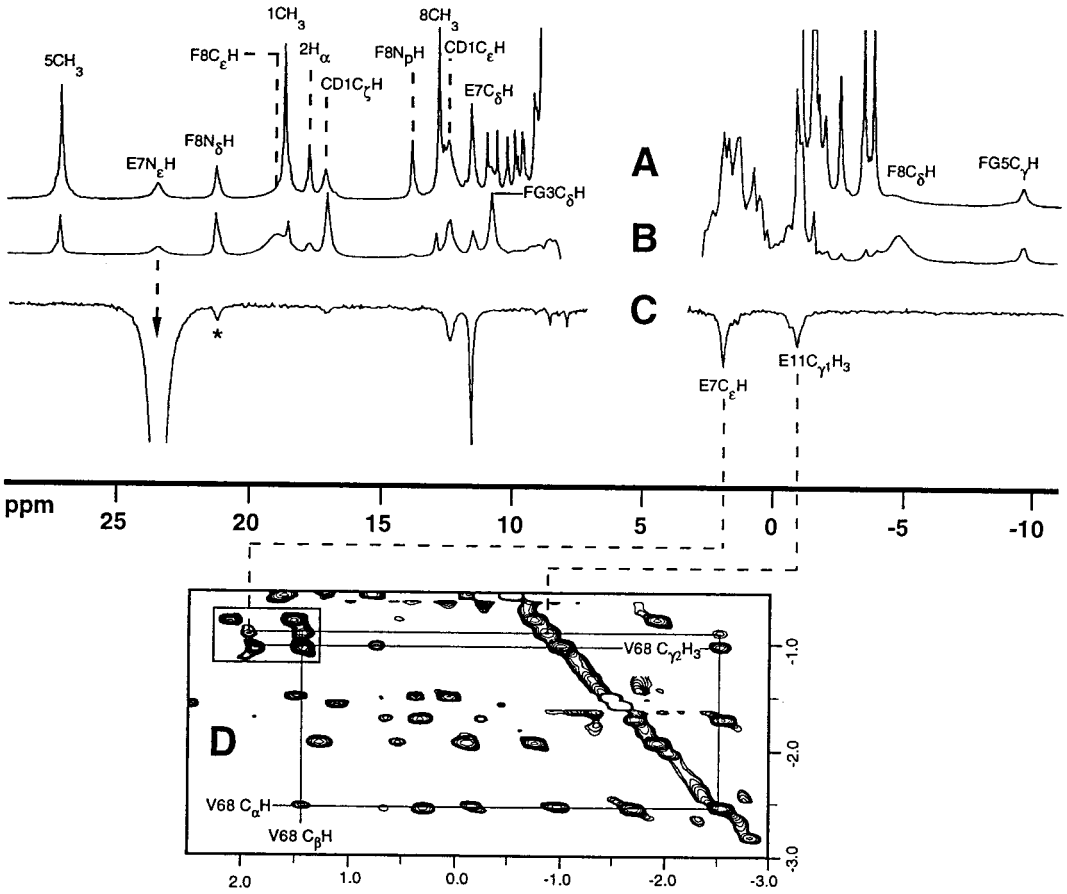

Figure 2. Portions of: (A) the normal 500 MHz ^{1}H NMR reference spectrum of metMbCN in ^1H_2O with labeling of the assigned resolved resonances; (B) WEFT ^{1}H NMR spectrum (relaxation delay, 120 ms; repetition time 300 ms) of metMbCN that emphasizes strongly relaxed lines and strongly suppresses the intensity of the diamagnetic envelope in the 0−5 ppm spectral window; (C) steady-state WEFT-NOE difference spectrum upon saturating the assigned His64(E7) $N_\epsilon H$ resonance, with each detected (and expected) NOE labeled by the residue and proton origin; (D) portion of the NOESY spectrum (50 ms) showing the expected dipolar connection between the newly assigned His64(E7) $C_\epsilon H$ and Val68(E11) $C_{\gamma 2}H_3$.

30% from the optimized value at 25 °C, followed by reoptimizing the other four parameters, results in a much larger residual $F/n = 0.26$, and to *large systematic deviations* of the observed from the calculated dipolar shifts (not shown, see Supporting Information). Last, a plot of δ_{dip}(calcd) vs δ_{dip}(obsd) specifically for the protons which exhibit either large or dominant rhombic dipolar shifts also exhibits an excellent correlation (shown in Supporting Information).

Temperature Dependence of Magnetic Properties. The results of carrying out the five-parameter least-squares searches using the 26 dipolar shifts in set VT over the temperature range 5 to 50 °C also resulted in excellent correlation between δ_{dip}(obsd) and δ_{dip}(calcd), as shown in Figure 3B−D. The effect of temperature on $\Delta\chi_{ax}$ and $\Delta\chi_{rh}$ is shown in Figure 5A, which also includes the previously reported[11,46] theoretical values of the former, shown as a solid line. The effect of temperature on the Euler angles is included in Figure 5C−E. The value of α and β appear to decrease very slightly with temperature, but the changes are only marginally outside the error limits.

Temperature Dependence of Contact Shifts. The use of the δ_{dip}(calcd) over the temperature range 5−50 °C allows the determination of δ_{con}(calcd) according to eqs 1, 3, and 6 for the axial His and heme methyl and meso-H signals. The separation of the shifts into their contact and dipolar contributions at 25 °C is shown in Table 1. In each case, the uncertaintities in δ_{dip}(calcd) at 25° translate to uncertainties in δ_{con}(calcd). Curie plots of δ_{hf}(obsd) and δ_{con}(calcd) for the heme methyls determined on the basis of the experimental δ_{dip}(calcd) in the 5−50 °C range are shown in Figure 6A and B, respectively (dashed lines). In Figure 6B, we also show the plot of δ_{con}(calcd) based on an assumed strict T^{-1} dependence for δ_{dip}(calcd) imposed on the δ_{dip}(obsd) at 25 °C (solid line). The temperature dependence for δ_{con}(calcd) for the His93(F8) $C_\epsilon H$, the only proton with sizable contact shift (Table 1) for which the temperature dependence could be reasonably well defined, is included in Figure 5B, where we also show the predicted[11] behavior of the contact shift via χ/g.

Axial His Shifts in metMbCN Mutants. Detailed assignments for the axial His resonances of a variety of sperm whale single, double, and triple point mutants have shown[25,26] that the axial His signals, like the nonligated residue protons, exhibit dramatic shift ranges of 2−3 ppm for $C_\alpha H$ and C_βHs, ∼5 ppm for $N_\delta H$, and ∼25 ppm for both $C_\epsilon H$ and $C_\delta H$. Moreover, analysis of the δ_{dip}(obsd) for the structurally conserved, nonligated proximal side residues had, in each case, afforded[25,26] a set of magnetic axes for each metMbCN mutant in a manner similar to that described above (the relevant data are tabulated in Supporting Information). A plot of δ_{dip}(calcd) versus δ_{hf}(obsd) for the axial His93(F8) resonances for these 16 metMbCN mutants[25,26] is shown in Figure 7. In each case the data points show a reasonable correlation and are approximated by the straight lines through the data points. The apparent intercept in

(46) The anisotropy units in ref 11 are converted to SI units by multiplying by 4π.

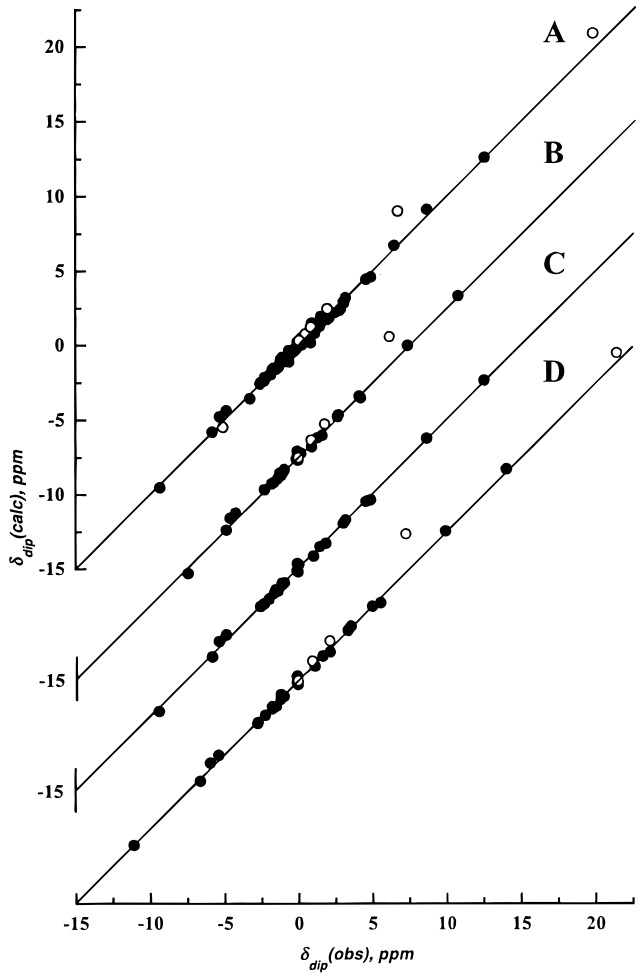

Figure 3. Plot of δ_{dip}(obsd) versus δ_{dip}(calcd) determined by the magnetic axes determinations: (A) using the most complete and reliable input data set PD3 with 87 input points at 25 °C, and using the input data set A at (B) 50 °C, (C) 25 °C, and (D) 5 °C. The input data are shown by solid markers. Also included in each case are the data for the His64(E7) ring (open marker) whose orientation in metMbCN may differ slightly from that in the reference MbCO structure.

Figure 7 at δ_{dip}(calcd) = 0, which should represent δ_{con} for each proton for His93(F8), is defined as $\delta^*_{con}(T^{-1} = 0)$, and the values for the His93(F8) protons are listed in Table 1.

Discussion

Definition of the Paramagnetic Susceptibility Tensor. The results of five-parameter least-squares searches for $\Delta\chi_{ax}$, $\Delta\chi_{rh}$, α, β, and γ for 16 different input data sets ranging from only six input shifts (C1) lead to highly clustered values for all parameters. A graphic representation of these results is given in Figure 4. The only data set that deviates significantly from any of the others is set N1 (proton helices with $R_{Fe} < 8$ Å), which has only six experimental data points and is dismissed as inadequate. For the remaining data sets, neither the size of the data set nor its localization (proximal, distal, near, remote) produced significant changes in any of the parameters, arguing against significant mobility of side chains and/or loops in biasing the magnetic axes determination. The failure to detect any bias based on proton distance to the iron or location on either helix or turn suggests that the crystal structure represents an adequate representation of the mean solution structure.

Most accurately defined is $\Delta\chi_{ax}$, which exhibits a total range $(2.58 \pm 0.09) \times 10^{-8}$ m^3/mol (±4%) for all data with more than 10 input points, and 2.58 ± 0.10 (±2%) for the most complete data set PD5. Combining range and uncertainty bounds $\Delta\chi_{ax}$ at $(2.58 \pm 0.10) \times 10^{-8}$ m^3/mol (±5%). Although $\Delta\chi_{rh}$ has a range for different input sets and an uncertainty per set that is comparable to that for $\Delta\chi_{ax}$, its smaller value leads to a less well-defined value with $\Delta\chi_{rh} = (-0.60 \pm 0.10) \times 10^{-8}$ m^3/mol (±16%) m^3/mol for all searches, which improves to -0.60 ± 0.05 (~8%) for the more extensive PD5 input data set. In general, the uncertainty in each determined value decreases sharply with the size of the data set without a significant change in the value. The value for $\Delta\chi_{ax}$ deduced here is smaller (by ~8%) than the theoretical estimate,[11,46] and slightly larger (by ~8%) than that estimated on the basis of less complete data sets.[47,48] Our conclusions here are that the accuracy in the $\Delta\chi_{ax}$ determination using the most comprehensive and reliable data set is such so as to eliminate the possibility that its value is 30% less than that reported previously, a value that was suggested[29] would invalidate an analysis[28] of residual dipolar contribution to $^{15}N-^{1}H$ coupling constants in terms of helical mobility in a partially oriented metMbCN. Moreover, a 30% change in $\Delta\chi_{ax}$ led to plots of δ_{dip}(obsd) vs δ_{dip}(calcd) which exhibited large and systematic deviations from the unit slope which were minimally improved by optimizing the remaining four parameters (not shown; see Supporting Information). Last, the 2.2 ppm δ_{dip}(obsd) for Leu29(B10) $C_\alpha H$, which is 9.2 Å from the iron, alone demands a $\Delta\chi_{ax} > 2.0 \times 10^{-8}$ m^3/mol.

The tilt, β, of the major axis from the heme normal exhibits a range $15.9 \pm 0.5°$ for all data sets and $15.9 \pm 0.3°$ for the most complete PD5 intput data and is the most accurately determined Euler angle. In contrast, α, the direction of the tilt of the major magnetic axis[37] when projected on the heme plane, exhibits a wider range, $150 \pm 8°$, for all valid input sets so that the uncertainty per set extends to $150 \pm 10°$; the range is only moderately imporved for the more complete PD sets to $151 \pm 5°$. The lower uncertainties, with minor variation in mean, with increased size of data set are particularly evident for the more complete PD set. Last, while both α (±10°) and γ (±10°) exhibited ranges of values with the particular data sets, the sum, $\kappa = \alpha + \gamma$, which represents the projection of the rhombic axes on the heme plane,[37] exhibits uncertainties (±10°) which are also less than the sums of those for α and γ. The Euler angles are within the uncertainties of values reported on the basis of less complete data sets[10,14,47,48] and confirm the previous estimates of uncertainties in α, β, κ of ±1, ±10, ±10°, respectively, based primarily on the sensitivity of the error function to the variations in these angles. The poorer definitions of $\Delta\chi_{rh}$ and κ result largely from the fact that the heme occupies most of the space significantly influenced by these two parameters and hence is an intrinsic limitation of this approach. It is noted, however, that the correlation between δ_{dip}(obsd) and δ_{dip}(calcd) for protons with large contributions from $\Delta\chi_{rh}$ (either as magnitude or as fraction of total dipolar shift) correlate as well as do the remainder of the data (not shown, see Supporting Information).

Last, while the His64(E7) ring protons were not used as input in the magnetic axes determinations, the observed dipolar shifts are well-predicted (open marker, Figure 3) at all temperatures, indicating that the major difference for the His64(E7) ring in metMbCN relative to MbCO[15] is the rearrangement of the labile

(47) Banci, L.; Pierattelli, R.; Turner, D. L. *Eur. J. Biochem.* **1995**, *237*, 522−527.

(48) The anisotropy units in ref 47 are converted to molar anisotropies by mulitplying by N_A.

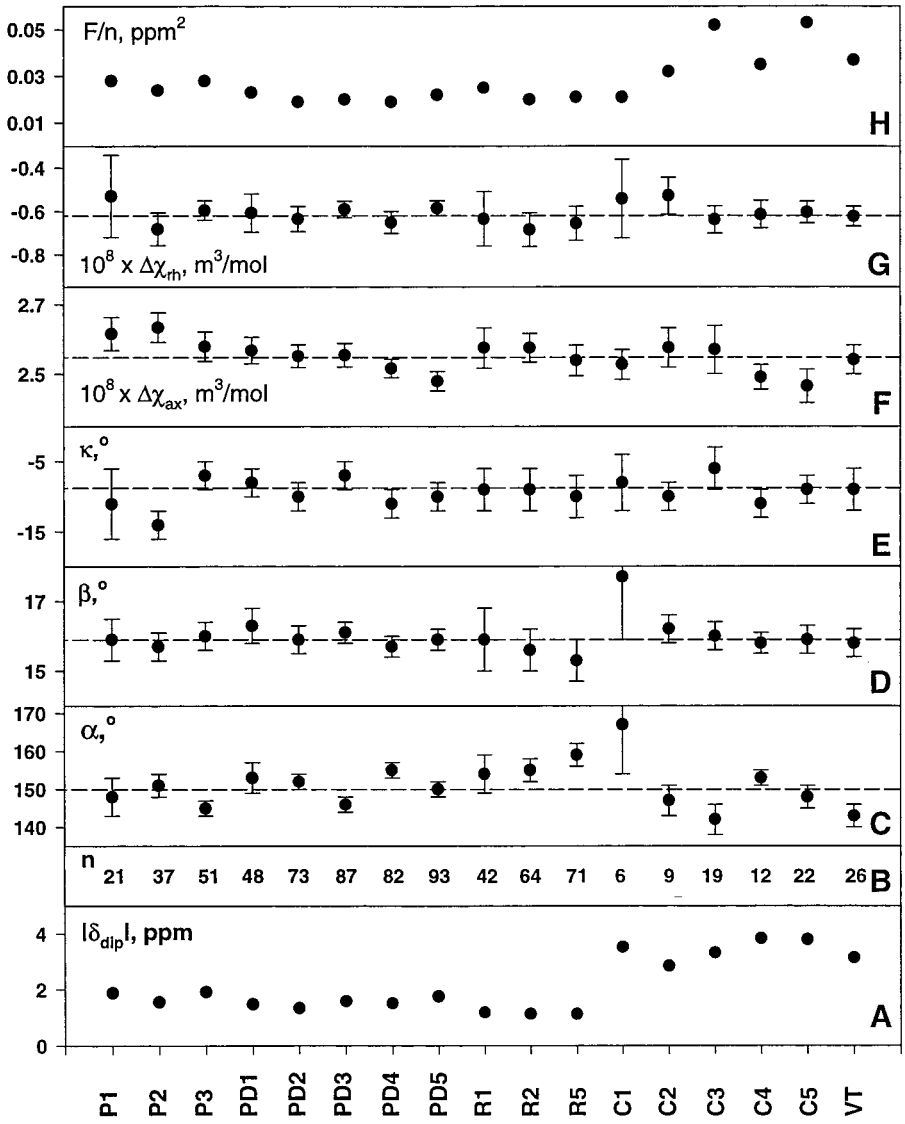

Figure 4. Graphic representation of the mean absolute input dipolar shift (A), the number of input data points (B), the Euler angles[37] and their uncertainties, α (C), β (D), and $\kappa = \alpha + \gamma$ (E), the axial (F) and rhombic (G) anisotropies[45] and their uncertainties, and the residual error function, *F*/*n* (H) resulting from five-parameter least-squares searches for the anisotropies and orientation of the paramagnetic susceptibility tensor of sperm whale metMbCN at 25 °C. The symbols at the bottom for the different input data sets represent: P, proximal protons; PD, both proximal and distal protons; R, protons remote from the iron (>8 Å); N, protons near the iron (≤8 Å), and 1, only helix backbone protons; 2, helix backbone and immobile side-chain protons; 3, set 2 plus the protons on the FG-corner; 4, set 2 plus protons on the CD corner; 5, set 2 plus protons on both the FG and CD corners; set VT is the reference data set used for the variable temperature study.

proton from the ring N_δ in the latter, to the ring N_ϵ in the former, as found[50] in MbO_2.

Temperature Dependence of Magnetic Axes. The experimental $\Delta\chi_{ax}$, $\Delta\chi_{rh}$, α, β, and κ as a function of temperature are shown in Figure 5, which also shows the theoretical lines[11,46] for $\Delta\chi_{ax}$. The robust nature of the magnetic axes is affirmed by the observation of a very regular temperature dependence to $\Delta\chi_{ax}$ that is defined by a straight line that bears remarkable similarity to that predicted for the system.[11] In accordance with predictions for metMbCN, $\Delta\chi_{ax}$ exhibits a temperature dependence in the experimental accessible temperature range with a significant negative apparent intercept. This negative intercept has been shown[11] to result from an essentially temperature-dependent second-order Zeeman (SOZ) contribution that is of the opposite sign as the temperature dependence first-order Zeeman (FOZ) contribution. The close parallel in both the magnitude and temperature dependence of $\Delta\chi_{ax}$ between the experimental and theoretical results serves to validate the results. The values of $\Delta\chi_{rh}$ over the same temperature range also lead to a well-defined straight line, despite larger uncertainties than for $\Delta\chi_{ax}$, as shown in Figure 5A. The plots of the fractional changes in both $\Delta\chi_{ax}$ and $\Delta\chi_{rh}$, normalized to the value at 25 °C, are shown as dash-dot-dash-dot lines for $\Delta\chi_{ax}$ and dash-dot-dot lines for $\Delta\chi_{rh}$ and show that the magnitude of $\Delta\chi_{rh}$ *decreases fractionally much more rapidly* than either the experimental or theoretical value for $\Delta\chi_{ax}$. Whereas the expected temperature behavior for $\Delta\chi_{rh}$ was not reported,[11] the smaller negative SOZ contribution relative to the positive FOZ for $\Delta\chi_{rh}$, when compared to $\Delta\chi_{ax}$, would lead to the expectation that $\Delta\chi_{rh}$ would exhibit less intrinsic "hyper-Curie" behavior than $\Delta\chi_{ax}$, in contrast to what is observed (Figure 5A).

The changes in Euler angle with temperature (6° for α, 0.6° for β, and 6° for κ), are surprisingly systematic, as shown in Figure 5C−E, but are in each case less than the uncertainties

(49) Cheng, X.; Schoenborn, B. P. *J. Mol. Biol.* **1991**, *222*, 381−399.

(50) Hanson, J. C.; Schoenborn, B. P. *Nature* **1981**, *53*, 117−146.

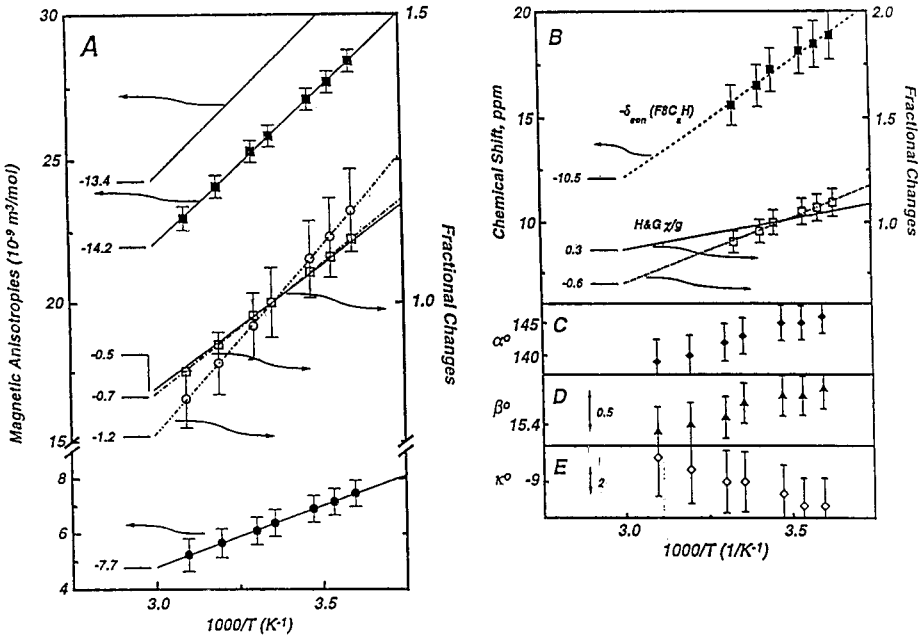

Figure 5. (A) Plot of the determined $\Delta\chi_{ax}$[45] (closed squares) and $(-)\Delta\chi_{rh}$ (closed circles) as a function of reciprocal temperature (Curie plot) obtained from five-parameter searches for the magnetic axes in the temperature range 5−50 °C. The solid line marked H-G represents the theoretical values for $\Delta\chi_{ax}$ reported by Horrocks and Greenberg.[11,46] The fractional changes with temperature (using the value at 25 °C as a reference) for the experimental anisotropies are shown for $\Delta\chi_{ax}$ (open squares) and $\Delta\chi_{rh}$ (open circles), and the theoretical value is shown by a solid line. (B) Experimental δ_{con}(calcd) for His93(F8) $C_\epsilon H$ (closed squares) as a function of temperature in a Curie plot determined as described in text. The solid lines represent the theoretical fractional change in contact shift in eq 2 as a function of temperature, normalized to 25 °C, and the dashed−dotted lines represent the fractional change in δ_{con}(calcd) as a function of temperature, normalized to 25 °C. The effect of temperature on the orientation of the magnetic axes,[37] α, β, $\kappa = \alpha + \gamma$ are shown in (C), (D), and (E), respectively.

Table 1. Separation of Contact and Dipolar Shifts for the Heme and Axial His93(F8) in MetMbCN[a]

	δ_{DSS}(obsd)[a]	δ_{DSS}(dia)[b]	δ_{hf}(obsd)[c]	δ_{hf}(int)[d]	δ_{dip}(calcd)[e]	δ_{con}(calcd)[f]	δ_{con}(int)[g]	δ^*_{con}[h]
heme								
1-CH_3	18.55	3.63	14.92	−4.2	−3.2 ± 0.2	18.0 ± 0.2	−6.8	
3-CH_3	4.76	3.79	0.97	12.1	−5.0 ± 0.2	6.0 ± 0.2	11.7	
5-CH_3	27.07	2.53	24.54	−6.1	−3.0 ± 0.2	27.5 ± 0.2	−8.6	
8-CH_3	12.88	3.59	9.29	1.0	−5.4 ± 0.2	14.7 ± 0.2	−2.4	
α-meso-H	4.37	9.92	−5.55	0.3	−12.1 ± 0.5	6.6 ± 0.5	0.6	
β-meso-H	2.09	9.34	−7.25	7.7	−10.1 ± 0.4	2.8 ± 0.4	−1.3	
γ-meso-H	5.98	10.15	−4.17	1.3	−10.5 ± 0.4	6.3 ± 0.4	0.9	
δ-meso-H	4.05	9.86	−5.81	4.4	−11.9 ± 0.5	6.1 ± 0.5	−6.2	
His(F8)								
NH	13.88	7.15	6.73	−4.1	5.5 ± 0.1	0.9 ± 0.1	−0.4 ± 1.0	
$C_\alpha H$	7.47	2.90	4.57	−1.4	4.6 ± 0.1	0.01 ± 0.1	0.8 ± 0.3	
$C_{\beta 1} H$	11.59	1.55	10.04	−3.4	6.6 ± 0.2	3.4 ± 0.2	−1.6	2.6 ± 1.2
$C_{\beta 2} H$	6.35	1.72	4.63	−0.4	3.9 ± 0.2	0.8 ± 0.2	−1.7	0.9 ± 0.3
$N_\delta H$	21.31	9.36	11.95	−7.6	15.4 ± 0.3	−3.5 ± 0.3	0.4	−6.8 ± 1.6
$C_\delta H$	−4.78	1.13	−5.91	8.6	−4.8 ± 0.8	−1.1 ± 0.8	−16.1	−2.5 ± 0.8
$C_\epsilon H$	18.98	1.66	17.32	−24.3	36.6 ± 1.0	−19.3 ± 1.0	10.5	−14.1 ± 1.6

[a] Shifts in ppm at 25 °C, in ^2H_2O, pH 8.6. [b] Diamagnetic chemical shift for MbCO.[38] [c] Hyperfine shift given by eq 6. [d] Intercept, in ppm, at $T^{-1} = 0$ in a plot of δ_{hf}(obsd) versus T^{-1} (Curie plot). [e] Determined by eq 3 and magnetic axes for data set PD3. [f] Contact shift obtained from eq 1 and eq 6. [g] Intercept at $T^{-1} = 0$ in a plot of δ_{con}(calcd) versus T^{-1} (Curie plot). [h] Intercept at δ_{dip}(calcd) in a plot of δ_{hf}(obsd) versus δ_{dip}(calcd) for the His F8 protons in 16 point mutant MbCN complexes.[25,26]

for the VT data set, and hence, it can be concluded that the structure of the heme cavity is not significantly altered in the temperature range. These results are consistent with the minimal structural changes observed in the 298 and 77 K crystal structures.[51] The well-defined anisotropies and Euler angles and the adherence of these parameters to changes in temperature along with expectations for a well-defined solution structure lead us to conclude that ^1H NMR has considerable promise in determining the anisotropy and orientation of the paramagnetic susceptibility tensor in low-spin ferrihemoproteins.

(51) Frauenfelder, H.; Hartmann, H.; Karplus, M.; Kuntz, I. D., Jr.; Kuriyan, J.; Parak, F.; Petsko, G. A.; Ringe, D.; Tilton, R. F., Jr.; Connolly, M. L.; Max, N. *Biochemistry* **1987**, *26*, 254−261

Heme and Axial His Contact Shifts. The ability to quantitatively describe the dipolar shifts for 96 protons which exhibit only δ_{dip} allows us to quantitatively predict δ_{dip} for the heme methyl, meso, and axial His(F8) protons, as shown in Table 1. Consistent with earlier considerations,[12] the heme methyl shift pattern is indeed dominated by the contact shift, and the pattern of contact shifts among the four methyls is similar to that for the total hyperfine shifts, except that the opposite sign of δ_{con} and δ_{dip} leads to less fractional asymmetry in the apparent spin distribution (see below) than apparent in δ_{hf}(obsd), as observed in the Curie plots in Figure 6. Of more interest is the result that each of the *meso-H's clearly exhibits significant low-field contact shifts*, as was suggested earlier on the basis of much more

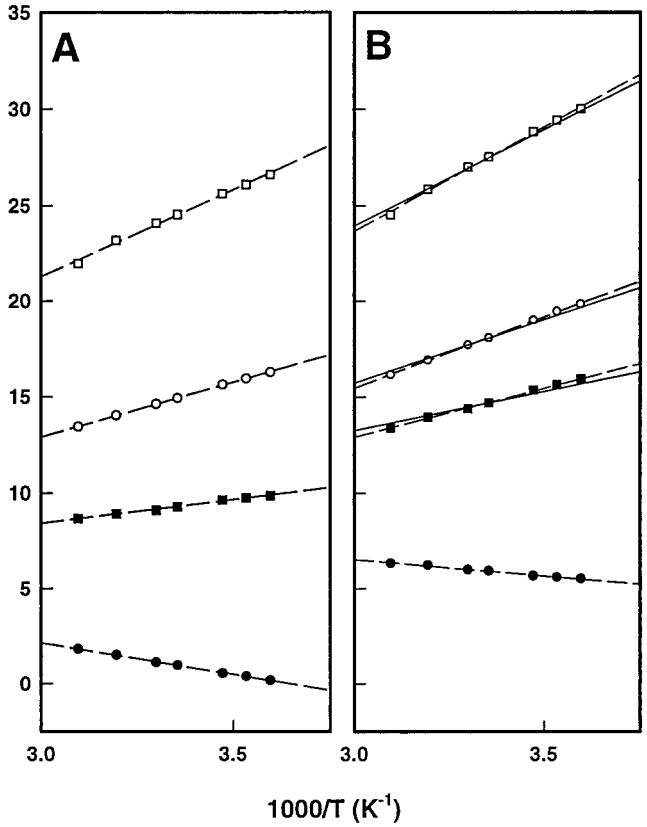

Figure 6. Curie plots for the heme methyls in metMbCN: (A) δ_{hf}-(obsd) (dashed lines) and (B) δ_{con}(calcd) obtained via eqs 1 and 6 using the experimentally determined temperature dependence for δ_{dip}(calcd) (dashed lines). The solid line in (B) shows δ_{con}(calcd) obtained via eq 5 of the δ_{dip}(calcd) at 25 °C as forced to exhibit true Curie behavior ($\propto T^{-1}$ with zero intercept) (1-CH_3, open circle; 3-CH_3, closed circle; 5-CH_3, open square; 8-CH_3, closed square) of metMbCN.

primitive approaches to separation of δ_{dip} and δ_{con} in model complexes.[7,52] The porphyrin 3e(π) MOs[7,8] have significant coefficients at the pyrrole carbons but exhibit nodes at the meso-carbon. The lowest vacant 4e(π) MOs could be expected to weakly interact with d_π orbitals;[7,8] however, this would lead to significant *upfield* meso-H contact shifts, contrary to observation. One possible origin of this low-field meso-H contact shift is some σ-spin delocalization due to the fact that the large tilt ($\sim$16°) of the major magnetic axis eliminates the σ/π separation of the d orbitals and could make the spin containing d_{xz} or d_{yz} orbitals weakly σ-bonding. The other possibility is that σ/π separation is lost due to the commonly observed deformation of the heme from planarity. In any case, the origin of contact shifts for the meso-H from a mechanism other than π spin density in the 3e(π) MOs of the heme could have serious consequences for the interpretation of the anomalous temperature dependence of the heme methyl contact shifts in terms of the energy separation between the d_{xz} and d_{yz} orbital holes (see below).

Separation of δ_{con} and δ_{dip} for the axial His93(F8) demonstrates that δ_{hf} for both $C_\alpha H$ and N_pH are essentially dipolar, a conclusion that is consistent with the expectation that π spin delocalizations have no effective mechanism for extending beyond the β-carbon of the ligated His.[6] The δ_{con} values for His93(F8) show that the π spin density is primarily at $C_\epsilon H$, where it induces the expected large upfield δ_{con}, as noted previously for axial His in a variety of low-spin ferrihemoproteins.[19] A lesser amount of π spin density manifests itself at the C_γ, where it induces the expected smaller *upfield* $C_\beta H$ contact shift; the relative magnitude of the $C_{\beta 1}H$ and $C_{\beta 2}H$ δ_{con} is consistent with the known orientation relative to the imidazole plane.[53] The data in Figure 5B show that the His(F8) $C_\epsilon H$ contact shift exhibits strong hyper-Curie behavior.

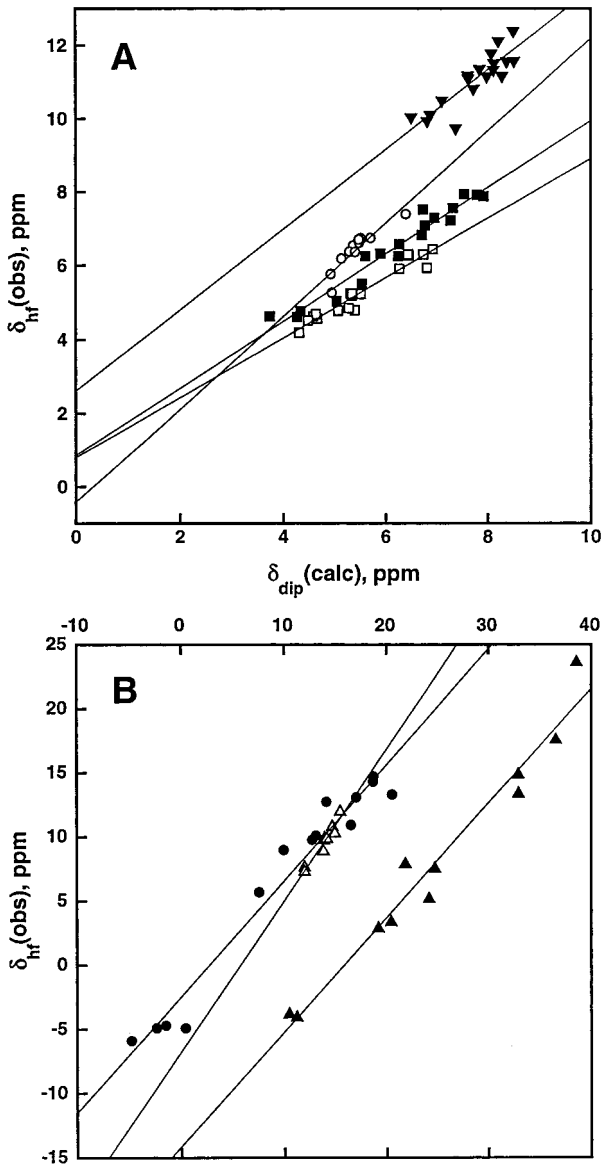

Figure 7. Plot of δ_{dip}(calcd) versus δ_{hf}(obsd) for (A) N_pH (open circles), $C_\alpha H$ (open squares), $C_{\beta 1}H$ (closed triangles) and $C_{\beta 2}H$ (closed squares) and (B) imidazole ring $N_\delta H$ (open triangles), $C_\delta H$ (closed circles), and $C_\epsilon H$ (closed triangles) of the His93(F8) in 16 metMbCN mutants for which the magnetic axes for those have been determined and reported.[25,26] The data points for each proton can be fit to a line whose intercept (defined as $\delta^*_{con}(T^{-1} = 0)$) at δ_{dip}(calcd) = 0 should correspond to δ_{con}. The values of δ^*_{con} ($T^{-1} = 0$) are listed in Table 1. The identity of the mutants and the tabulated data are provided in Supporting Information.

The robust nature of the δ_{con} and δ_{dip} separation is strongly supported by the fact that δ_{con} values for the axial His(F8) obtained by this manner for WT metMbCN are the same, within experimental uncertainty, as derived from the intercepts of δ_{dip}-(calcd) vs δ_{hf}(obsd) (Figure 7) (defined δ^*_{con} in Table 1) for

(52) Satterlee, J. D.; La Mar. G. N. *J. Am. Chem. Soc.* **1976**, *98*, 2804−2808.

(53) The contact shift for a methylene proton that senses unpaired spin π density is $\propto \cos^2 \psi$, where ψ is the angle between the p_z axis and the H−C−C plane;[6] the values ψ, $\sim$30° and 77° for $C_{\beta 1}H$ and $C_{\beta 2}H$, respectively, correctly predict the much larger contact shift for $C_{\beta 1}H$.

16 sperm whale single, double, and triple mutants[25,26] for which highly varied orientation in the major magnetic axis induces a large range of shifts for the axial His. The strong similarity of the axial His δ_{con} values obtained in these two procedures shows that the highly variable hyperfine shifts with mutations for both the axial His and the nonligated residues in metMbCN complexes can be explained by a single, consistent interpretative basis with a conserved contact shift (i.e., conserved Fe−His π-bonding) with mutation and with primarily *the orientation of the major magnetic axis modulated* among the various distal mutants.

Relevance to the Spacing for the Orbital Excited State. A simplistic picture for the electronic/magnetic properties of the low-spin hemin/His chromophore with the His oriented along the N−Fe−N vectors through pyrroles B and D would have $\Delta\chi_{ax}$ conserved for the ground $(d_{xy})^2(d_{xz})^2(d_{yz})$ and excited $(d_{xy})^2(d_{yz})^2(d_{xz})$ orbital states and $\Delta\chi_{rh}$ rotated by 90° (*i.e., a change of sign*) between the two states.[54] The ground (d_{yz} hole) state, moreover, would exhibit large pyrrole A(1-CH_3) and C(5-CH_3), negligible pyrrole B(3-CH_3) and D(8-CH_3) contact shifts and large His F8 contact shifts, while the excited (d_{xz} hole) state would display large contact shifts for pyrrole B(3-CH_3), D(8-CH_3), but none for either pyrroles A(1-CH_3), C(5-CH_3) or the axial His. For the case where the energy spacing between the d_{xz} and d_{yz} orbital holes is comparable to *kT*, and we assume strict Curie behavior for both δ_{dip} and δ_{con} for a single orbital state, raising the temperature to populate the excited state should lead to: (1) hyper-Curie (apparent intercept of opposite sign to the shift) and hypo-Curie (large intercept of the same sign as the shift in a Curie plot) for methyls of pyrrole A, C and pyrrole B, D, respectively; (2) a strong hyper-Curie behavior for the axial His(F8) δ_{con}, with intercept of opposite sign to the shift; and (3) hyper-Curie behavior for the effective $\Delta\chi_{rh}$. Inspection of Figures 5A,B and 6 reveals that this is *qualitatively* the behavior shown by metMbCN for the heme methyls, His F8 $C_\epsilon H$ contact shift, and $\Delta\chi_{rh}$. Thus, all three manifestations of the expected effect of thermal population of the excited orbital state are clearly observed. More ambiguous, however, is the route for making qualitative estimates to ΔE.

The observed "anomalous" temperature behavior related to population of the excited state could be interpreted in terms of the magnitude of the orbital spacing which, in turn, could provide detailed information on the axial His−Fe bond strength. There are several factors, however, which preclude at this time such a meaningful interpretation for the globins. First, the temperature dependence for both δ_{con} and δ_{dip} are predicted[11] to be non-Curie for a given state, and the present study generated experimental data to substantiate this fact. It is readily apparent that the correction of δ_{hf} (Figure 6A) for δ_{dip} with strict Curie (Figure 6B, solid lines) and the experimental temperature dependence on δ_{dip} (Figure 6B, dashed lines) alters the degree of "hypo"- and "hyper"-Curie behavior for the methyl δ_{con}, and would lead to different estimates of ΔE. Second, the heme meso-H's exhibit contact shifts that are consistent with *dominant* σ delocalized spin. This could result either from the breakdown of σ/π separation for d_{xz}, d_{yz} from significant tilt of the major magnetic axis from the heme normal or from the known deformation of the porphyrin atoms from a plane. Thus, such σ spin density likely also contributes to the methyl contact shift, and the temperature of the π and σ contribution to the methyl contact shifts would be expected to differ. Last, the pattern of heme methyl contact shifts shows less asymmetry than that expected from a His F8 ring oriented within 5° of the N−Fe−N vector,[16] and the $\kappa = -8°$ determined herein is not consistent with the $\kappa = +5°$ predicted[55] by the counter-rotation rule and observed in models,[52,56] and suggests that the orbital hole is not determined solely by the axial His. This latter effect would lead to a decrease (increase) in δ_{con} for the axial His F8 in the ground (excited) orbital state. Potential contributions to the location of the rhombic axes are the ubiquitous vinyl groups which can conjugate with the heme and resolve the contact shift degeneracy of the four methyls even in a model with axially symmetric ligands[57] and the strong π contacts of the heme with the ubiquitous Phe43(CD1) and His97(FG3) in mammalian globins. Solution NMR characterization of metMbCN complexes reconstituted with appropriate chemically modified hemin and point mutants designed to perturb aromatic heme contacts are in progress.

Acknowledgment. This research was supported by a grant from the National Institutes of Health, HL 16087.

Supporting Information Available: Four figures (fingerprint NOESY/TOCSY spectra, δ_{dip}(obsd) vs δ_{dip}(calcd) for δ_{dip} dominated by $\Delta\chi_{rh}$; shift temperature gradient vs δ_{dip}(obsd); δ_{dip}(obsd) vs δ_{dip}(calcd) as a function of temperature) and six tables (δ_{DSS}(obsd), δ_{dip}(obsd), δ_{dip}(calcd)), magnetic axes, protons with large $\Delta\chi_{rh}$ contribution, temperature dependence of heme shifts and magnetic axes, input data for magnetic axes (19 pages, print/PDF). See any current masthead page for ordering information and Web access instructions.

JA982555O

(54) Shokhirev, N. V.; Walker, F. A. *J. Am. Chem. Soc.* **1998**, *120*, 981.

(55) Oosterhuis, G.; Lang, G. *Phys. Rev.* **1969**, *178*, 439−456.

(56) Byrn, M. P.; Katz, B. A.; Keder, N. L.; Levan, K. R.; Magurany, C. J.; Miller, K. M.; Pritt, J. W.; Strouse, C. E. *J. Am. Chem. Soc.* **1983**, *105*, 4916−4922.

(57) Cavaleiro, J. A. S.; Rocha Gonsalves, A. M. d'A.; Kenner, G. W.; Smith, K. M.; Shulman, R. G.; Mayer, A.; Yamante, T. *J. Chem. Soc., Chem. Commun.* **1974**, 392.